Review article **Open Access**

Xingshu Sun, Yubo Sun, Zhiguang Zhou, Muhammad Ashraful Alam and Peter Bermel*

Radiative sky cooling: fundamental physics, materials, structures, and applications

DOI 10.1515/nanoph-2017-0020
Received February 3, 2017; revised March 31, 2017; accepted April 5, 2017

Abstract: Radiative sky cooling reduces the temperature of a system by promoting heat exchange with the sky; its key advantage is that no input energy is required. We will review the origins of radiative sky cooling from ancient times to the modern day, and illustrate how the fundamental physics of radiative cooling calls for a combination of properties that may not occur in bulk materials. A detailed comparison with recent modeling and experiments on nanophotonic structures will then illustrate the advantages of this recently emerging approach. Potential applications of these radiative cooling materials to a variety of temperature-sensitive optoelectronic devices, such as photovoltaics, thermophotovoltaics, rectennas, and infrared detectors, will then be discussed. This review will conclude by forecasting the prospects for the field as a whole in both terrestrial and space-based systems.

Keywords: radiative cooling; nanophotonics; selective thermal emission; photovoltaics; infrared detectors; thermophotovoltaics; emissive energy harvesters.

1 Introduction

Radiative cooling is a strategy to dissipate excess heat into remote heat sinks (such as the clear sky) via thermal radiation [1]. Its crucial value is that it can lower the operating temperature of a broad range of solid-state devices without requiring any input energy. It functions on the ground by enhancing radiation at wavelengths that are highly transmitted [2]; for the sky, this transparency window extends from 8 to 13 μm [3]. The earliest adoption of radiative cooling has been traced back to the courtyard architectures of ancient Iran [4]. In the modern era, the first scientific studies found that certain materials have potential for limited selectivity, notably polymeric materials [5, 6], titanium dioxide [7–9], silicon nitrides [10], and silicon monoxide (SiO) [11]. While cooling to 40°C below ambient with SiO is theoretically possible [11], the temperature difference is much smaller in experiments [2]. Although the natural materials listed above can enhance radiative cooling, achieving the best possible radiative cooling requires a combination of high and flat emittance throughout the sky transparency window. No simple bulk material has been reported to provide this ideal emittance spectrum, and thus, theoretically maximal radiative cooling power.

Fortunately, with the emergence of new classes of selective infrared (IR) emitters [12–14], based on photonic design principles [15], interest in radiative cooling has increased substantially in the last several years. Recent calculations first indicated, for instance, that 2D nanophotonic structures can provide a cooling power in excess of 100 W/m^2 at reasonable temperatures [16]. A 1D stack of hafnia and silica, consisting of seven bilayers, was shown to be sufficient to achieve cooling below ambient temperatures in experiment [17]. Before this recent resurgence of interest, research efforts focused on looking for the best cooling material for below-ambient cooling at night. Most materials investigated previously were bulk materials or composite materials. Some were found to be satisfactory for nocturnal applications. However, the capability of daytime radiative cooling under direct sunlight, especially below ambient, was never fulfilled until very recently. The development of nanophotonics is certainly a major driving force behind the recent resurgence of radiative cooling research. It is found that minimal absorption of direct sunlight and high emittance within the atmospheric window can both

***Corresponding author: Peter Bermel,** Network for Photovoltaic Technology, School of Electrical and Computer Engineering, Purdue University, West Lafayette, IN 47907, USA; and Birck Nanotechnology Center, Purdue University, West Lafayette, IN 47907, USA, e-mail: pbermel@purdue.edu
Xingshu Sun, Yubo Sun and Muhammad Ashraful Alam: Network for Photovoltaic Technology, School of Electrical and Computer Engineering, Purdue University, West Lafayette, IN 47907, USA
Zhiguang Zhou: Network for Photovoltaic Technology, School of Electrical and Computer Engineering, Purdue University, West Lafayette, IN 47907, USA; and Birck Nanotechnology Center, Purdue University, West Lafayette, IN 47907, USA

be satisfied by nanophotonic designs. As will be discussed later in Section 3.3, the capability of daytime radiative cooling, compared with nighttime cooling, gives rise to more applications and research opportunities in different fields. In related work, it was shown that this approach can be applied to solar cells to theoretically achieve meaningful temperature reductions. Theoretically, the temperature for bare silicon cells can be up to 17.6°C in unconcentrated sunlight [18], with an actual 13°C cooling effect observed in experiment [19]. Similarly, despite their lower self-heating, GaAs nanowire-based photovoltaics (PV) could potentially experience a radiative cooling-induced temperature drop of 7°C [20], which could improve their performance by 2.6% absolute efficiency in the near-earth orbit [21]. For encapsulated commercial solar panels, the cover glass (typically soda-lime glass) is already a decent broad-band radiative cooler. Hence, a temperature decrease of only 1–2 K is achievable by radiatively cooling commercial solar panels, which surprisingly still can extend the lifetime significantly by suppressing thermally activated degradation [22].

The resulting drop in efficiency associated with excess heating can be tremendous, potentially, over 50% of the relative performance [23]; thus, it is critical to develop new strategies for cooling that are nearly or fully passive, as opposed to active, to preserve overall system efficiencies and to substantially decrease operating temperatures, improving performance for a wide range of devices. In the best case, this additional cooling power could result in below-ambient operation, potentially enabling significantly improved performance and reliability.

Given these significant benefits, it seems appropriate to consider what other systems could potentially benefit the most from this radiative cooling approach. The most appealing applications would presumably combine considerable self-heating and significant needs for energy efficiency. Within this group, solid-state electronics stand out as particularly relevant, since they can experience substantial radiative heating outdoors during the daytime, along with electric power injection and subsequent thermal dissipation. Concentrator photovoltaics (CPV) and thermophotovoltaics (TPV) are likely to see even greater benefits from these approaches than standard PV, because of their greater heat fluxes [24].

In the subsequent sections, we will develop a physics-based modeling framework to capture the energy balance observed in a realistic radiatively cooled system. It will allow us to first investigate the ideal case of radiative cooling, and then to consider a variety of cooling structures based on real materials, such as low-iron soda-lime glass, many of which take advantage of nanophotonic design principles. Next, we show the benefit of increasing the area of the radiative cooling element, given a suitable heat spreader, which can even facilitate below-ambient cooling. Afterward, a range of specific applications enabled by radiative cooling will be discussed, including solar PV, CPV, TPV, rectenna-based nighttime power generation, and IR detectors as well as other temperature-sensitive electronics. Finally, we will conclude by summarizing progress to date as well as our perspective on future prospects in the field, especially as they relate to nanophotonics.

2 Fundamental physics of radiative cooling

Two facts make radiative cooling an achievable and significant phenomenon. First, the mean tropospheric temperature is generally around 250 K, well below ambient in most regions of the earth throughout the year [25, 26], and thus may act as a cooling reservoir. Second, the atmospheric transparency window extends across a wavelength range of 8–13 μm [1, 2, 27, 28], allowing thermal emission from an emitting object to connect with the low-temperature troposphere. To fully understand radiative cooling, we will explain the fundamental physics of this process in this section. We begin with the fundamentals of radiative heat transfer, followed by the most relevant atmospheric physics, and conclude with the fundamentals of radiative cooling both above and below ambient temperatures.

2.1 Thermal radiation fundamentals

Thermal radiation fundamentally arises from random energy level transitions in matter. For any object with finite temperature, energy transfer is thus realized by the resulting emission of energy in the form of electromagnetic waves, which consist of finite quanta of energy, or photons. Based on these considerations, the temperature-dependent emission is given by Planck's law of blackbody radiation [29]:

$$I_{BB}(T, \lambda) = \frac{2\pi hc^2}{\lambda^5} \frac{1}{e^{\frac{hc}{\lambda kT}} - 1}, \tag{1}$$

where I_{BB} is the spectral irradiance per unit area per unit wavelength, h is Planck's constant, c is the speed of light, k is Boltzmann's constant, and T denotes the temperature in K. By integrating the spectral irradiance over area and the whole wavelength range, it can be found that the total

emitted power is proportional to the fourth power of the emitter temperature, as described by the Stefan-Boltzmann law:

$$P = \varepsilon A \sigma T^4, \tag{2}$$

where P is the total emissive power, A is the surface area of the emitting object, σ is the Stefan-Boltzmann constant, and $\varepsilon = \int_0^\infty d\lambda I_{BB} \int_0^{\pi/2} d(\sin^2\theta)\varepsilon(\theta, \lambda) / \int_0^\infty d\lambda I_{BB}$ denotes the averaged emittance of the object. Note that $\varepsilon(\theta, \lambda)$ is an angular and spectral dependent parameter as discussed in [1, 2, 17]. For an ideal blackbody emitter, $\varepsilon = 1$ for all angles and wavelengths. On a related note, Kirchhoff's law states that for arbitrary matter absorbing and emitting thermal radiation under thermal equilibrium, its emittance is equal to its absorptance. Recently, a more generalized form of Kirchhoff's law has been derived by Greffet et al. [30] that extends to any finite size object, including those with temperature variations across their surface. Hence, the emittance of an object is generally considered equivalent to the absorptance, which helps derive the atmospheric transmittance from the atmospheric emittance.

2.2 Tropospheric temperature and atmospheric transmittance

The temperature of the cosmic microwave background radiation is around 3 K [31], while the sun is approximately a blackbody at an effective surface temperature closer to 5800 K. This enormous temperature difference, combined with heat transfer in the upper atmosphere, gives rise to a complex, altitude-dependent temperature profile [32], featuring a tropospheric temperature of about 50 K below standard room temperature (300 K) [2], which can serve as a potential radiative heat sink for ground level cooling. The exact cooling strongly depends on geographic location and climate, thus requiring a detailed calculation [33]. For simplicity, we will focus on ground level cooling. Exchange with the troposphere on the ground is limited by the atmospheric absorption spectrum [2, 27, 28, 34–38], which features a strong water vapor absorption band centered around 6 μm and beyond 20 μm, as well as a carbon dioxide absorption band that peaks around 15 μm. These absorption bands leave behind an atmospheric transmission window from 8 to 13 μm. Equivalently, if we assume that the entire atmosphere is radiating at ambient temperatures (~300 K), the effective transmittance within the atmospheric window is far above zero, as depicted in Figure 1. Furthermore, the atmospheric emittance is

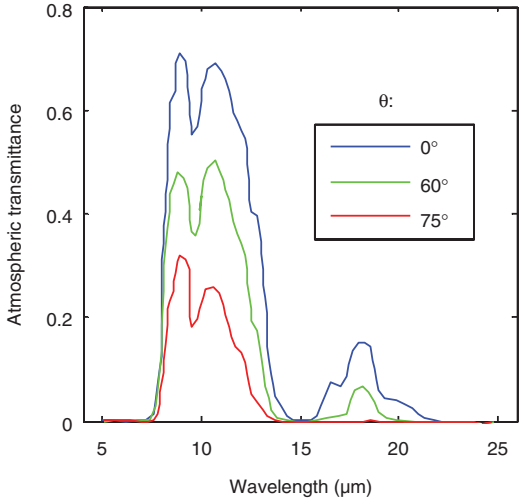

Figure 1: The atmospheric transmittance spectrum at zenith angles of 0°, 60°, and 75°; it is highest in the 8–13 μm transparency window. Results are adapted from [2].

not only wavelength dependent, but also zenith angle dependent, as expressed by the following equation [2]:

$$\varepsilon_a(\theta, \lambda) = 1 - [1 - \varepsilon_a(0, \lambda)]^{1/\cos\theta}. \tag{3}$$

Here $\varepsilon_a(\theta, \lambda)$ denotes the atmospheric emittance at any arbitrary zenith angle θ, based on Kirchhoff's law, equal to the atmospheric absorptance as well. On the other hand, because water vapor absorption dominates the atmospheric absorptance within the atmospheric window, the

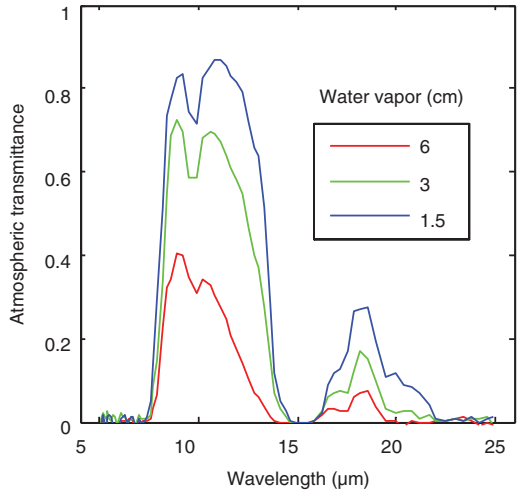

Figure 2: The computed atmospheric transmittance spectrum, computed using the Lowtran model. The temperature of the lowest kilometer of atmosphere is assumed to be 21°C, the ozone content assumed to be 0.35 atm · cm, and aerosols are of urban type with a 23 km visual range. Different precipitable water vapor levels are shown as red, green, and blue curves in the figure. These results have been adapted and replotted from [2].

transparency of the sky is quite sensitive to precipitable water vapor concentration, which is correlated with relative humidity (RH) and ground temperature [39, 40], and thus varies geographically. Its influence is illustrated in Figure 2: higher precipitable water vapor concentration leads to stronger absorption within the atmospheric window. Similarly, the atmospheric window dependence on RH was demonstrated in [41] by modeling transmittance characteristics during the summer solstice at two locations. The atmospheric transmittance within the 8–13 μm spectral window is higher in Perth than in Brisbane despite the close ambient temperatures, due to lower water vapor concentration in Perth than in Brisbane as reflected by the mean RH. In short, atmospheric transmission varies with geography in a well-understood manner.

2.3 Principle of cooling

Developing radiative coolers for various applications requires rigorous engineering and design. In this subsection, we review the physics of radiative cooling by the steady-state energy balance equation and summarize the design considerations for radiative coolers.

When a radiative cooler of surface area A is exposed to the sky, the cooling power P_{cool} here is the net outgoing radiative energy flux, which is given by

$$P_{cool}(T) = P_{rad}(T) - P_{atm}(T_{amb}), \tag{4}$$

where $P_{rad}(T) = A\int d\Omega \cos\theta \int_0^\infty d\lambda I_{BB}(T, \lambda)\varepsilon(\lambda, \theta)$ is the thermal emission of the radiative cooler with operating temperature of T, and $\int d\Omega \cos\theta$ is the integration of the solid angle over the hemisphere. The atmospheric radiation at a temperature T_{amb} is given by $P_{atm} = A\int d\Omega \cos\theta \int_0^\infty d\lambda I_{BB}(T_{amb}, \lambda)\varepsilon(\lambda, \theta)\varepsilon_{atm}(\lambda, \theta)$, where $\varepsilon_{atm}(\lambda, \theta)$ denotes the spectral and angular atmospheric emittance that can be calculated by Eq. (3). Balanced with other energy fluxes (e.g. incident solar power, convective, and conductive heat transfer), the maximum cooling power determines the lowest temperature achievable. Initially, nighttime radiative cooling appeared much more promising thanks to the absence of solar irradiance, and constituted the focus of the early work [42–46]. Enabled by recent advances in photonic design, daytime radiative cooling below ambient temperature has been demonstrated by Rephaeli et al. [16]. Such a cooling structure is engineered to be spectrally selective: (1) highly emissive between 8 and 13 μm to maximize $P_{rad}(T)$; (2) weakly emissive outside the atmospheric window to reduce parasitic radiation $P_{rad}(T_{amb})$; (3) either highly reflective or transparent in the solar spectrum to suppress sunlight absorption.

When designing a practical, efficient radiative cooling system, one must also consider other heat transfer pathways. Generally, the net power of the cooling system P_{net} is defined as

$$P_{net} = P_{cool} - P_{abs.sun} - P_{non-radiative}, \tag{5}$$

where P_{cool} denotes the radiative cooling power, $P_{abs.sun}$ is the total absorbed solar power only relevant for daytime applications, and $P_{non-radiative}$ corresponds to non-radiative heat transfer (i.e. convection and conduction). According to (5), solar absorption and non-radiative heat transfer act as parasitic cooling losses, thereby reducing the overall cooling efficiency and increasing the cooling time to reach thermal equilibrium. Remarkably, it has been experimentally demonstrated that significant temperature reduction up to 40 K below ambient has been reached by radiative cooling within 1 h [47]. For systems with greater heat loads (e.g. CPV and TPV), it is also expected that the temperature will quickly reach steady state due to significant heating, for example, temperature varies instantaneously with solar irradiance in [48]; in such cases, radiative cooling can still serve as a complementary passive cooling method to reduce overall system temperature. By eliminating those parasitic heat transfers, the lowest temperature achievable by radiative cooling is essentially the tropospheric temperature, which is ~50 K below ambient. Indeed, Chen et al. [47] have demonstrated a sub-freezing radiative cooling system with considerably reduced parasitic heat transfer (e.g. no convection in the vacuum chamber and Sun shade to block solar irradiance). The lowest temperature measured is 42 K below ambient, far lower than the previous under-optimized experimental demonstration [17].

2.4 Below-ambient cooling vs. above-ambient cooling

Radiative cooling can be categorized as either below-ambient or above-ambient, depending on specific applications. The target cooling temperature of a radiative cooler determines the desired spectral emittance profile; namely, a broadband cooler is needed for above-ambient cooling, while a selective cooler is needed for below-ambient cooling. The broadband cooler should have emittance close to one throughout the IR spectrum, and negligible absorptance in the solar spectrum for daytime cooling.

On the contrary, a spectrally selective cooler will have emittance close to one only in the atmospheric window (8–13 μm) and minimal emittance elsewhere. Next, we will interpret such design requirements into the temperature and spectrum dependence of $P_{cool}(T)$.

$P_{cool}(T)$ must be positive to ensure net cooling of a system. For above-ambient cooling (i.e. $T > T_{amb}$), the thermal radiation outside the atmospheric window from the cooler to the ambient (i.e. above-ambient cooling) becomes beneficial and adds up to higher total cooling power $P_{cool}(T)$; thus, a broadband design is preferable to deliver more cooling gain (see Figure 3). For below-ambient cooling (i.e. $T < T_{amb}$), parasitic thermal emission outside 8–13 μm from atmosphere heats up the cooler, resulting in a negative cooling power for the broadband. In contrast, a spectral selective cooler that can eliminate such undesired absorption of radiation from ambient and maximize $P_{cool}(T)$ is the best for below-ambient cooling. At $T = T_{amb}$, the net thermal radiation outside the 8–13 μm wavelengths from the coolers to the ambient becomes zero; essentially, both designs deliver the same cooling power (see the dashed lines in Figure 3). To summarize, cooler designs should be adopted for different cooling targets. Note that the calculation in Figure 3 only considers the primary atmospheric window from 8 to 13 μm, and has neglected the secondary atmospheric window that exists between 16 and 22 μm. Our simulation has shown that, with the presence of the secondary window, full-spectrum radiation coolers can generate 10–20 W/m^2 more cooling power than the selective radiative coolers only focusing on 8–13 μm. Consequently, the temperature range in which the selective radiative coolers (from 8 to 13 μm) are preferable needs to be at least ~5 K lower than the ambient instead of just below-ambient, which is in good agreement with Figure 1c in [47]. The secondary window, however, contributes only ~10% of the total cooling power at near-ambient temperature due to much lower transmittance (see Figures 1 and 2) and deviation from the wavelength range (i.e. around 10 μm) wherein IR blackbody radiation peaks. Since the impact of the secondary window on radiation cooling is fairly insignificant, it can be neglected in general. In the next section, we describe specific materials and structures that are suitable for either type of cooling.

3 Radiative cooling materials and structures

To achieve effective radiative cooling, cooling structures should have emittance spectra $\varepsilon(\theta, \lambda)$ that match the ideal specifications discussed in Section 2. Fortunately, emittance properties approaching these ideals can be found in bulk materials suitable for massive production. They have been extensively studied in pioneering works of the 1970s and 1980s [1, 2, 5, 6, 10, 11, 42, 51–57]. Similar to bulk materials, gaseous materials such as ethylene and ammonia have also been proposed to be radiative coolers [56, 58, 59]. Furthermore, several works also focused on using pigmented foils that are highly reflective in the solar spectrum and transparent in the atmospheric window, such that an underlying material can simultaneously cool itself via

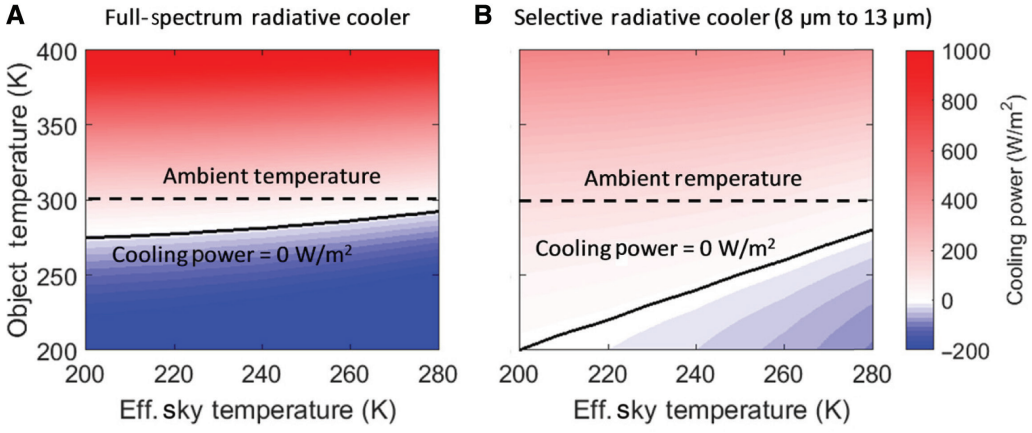

Figure 3: The net cooling power, as defined by Eq. (4), as a function of the object temperature and effective sky temperature for two cases: (A) a full-spectrum radiative cooler and (B) a selective radiative cooler. The horizontal dashed line indicates an ambient temperature of 300 K, and the black solid line illustrates zero cooling power. As in [49], sky radiation inside the atmospheric window is assumed to be emitted 3–5 km above ground at the effective sky temperature. The atmosphere is opaque outside the transparency window (8–13 μm). For realistic non-zero atmospheric transmittance outside 8–13 μm, full-spectrum radiative coolers may have slightly higher cooling power than selective radiative coolers (approx. 20 W/m^2) at ambient temperature [50].

thermal emission without absorbing solar irradiance [7, 9]. As the fabrication technique of nanomaterials advances, radiative coolers enabled by nanostructures and nanoparticles are proved to be good alternatives to bulk coolers [60, 61]. In recent years, nanophotonic structures have become powerful in tailoring the thermal emission properties of bulk materials [13, 62] and have a significant impact on different applications, including radiative cooling. It is demonstrated by simulation that properly designed photonic crystals (PhCs) can provide emittance spectra close to the ideal cases for radiative cooling (both above-ambient and below-ambient) under direct solar irradiance [16, 18, 63, 64]. Later, experiments successfully demonstrated the radiative cooling via PhC coolers [17, 19]. In addition to the spectral selectivity, the angular dependence of emittance is another important factor for radiative coolers, as implied in Eq. (4). Complete characterization of a radiative cooler should include its emittance spectra at multiple zenith angles. For cooling systems that are not angularly restricted, the emittance variation over zenith angles from 0° to 90° is preferred to be as small as possible [65]. It has recently been demonstrated that the weak angular dependence of emittance can be achieved by nanophotonic structures such as polymer stacks [66] and 2D PhC structures [19].

3.1 Bulk and gaseous material radiative coolers

In the early stage, plastic has been investigated as a prospective candidate for radiative coolers. Polyvinyl chloride (PVC) [5], polyvinyl fluoride (PVF) [1, 6, 42, 53, 54], and polymethylpentene (TPX) [52] were shown to have high emittance in the atmospheric window. Most plastic coolers reported in the literature were aluminized at the back to block transmission without adding significant absorption outside the atmospheric window. Although the TPX and PVF emittance spectra match the atmospheric window, as shown in Figure 4A [2, 52], TPX is slightly better, due to its higher emittance near 8 μm.

Alternative bulk materials, such as oxide and nitride, have been investigated extensively in the pioneering works of Granqvist et al. It was found that SiO, with its strong lattice absorption near 10 μm, can serve as a selective radiative cooler. The optimal thickness of 1 μm was found to be most effective in reducing reflection [2, 11]. Like the previous structure made from plastic coolers, an Al back reflecting layer was coated by evaporation [2, 11]. The structure and the reflectance of the SiO cooler are shown in Figure 4B [2]. However, the emittance of SiO within the atmospheric window is not strong enough to yield a significant improvement in the cooling effect compared with a blackbody cooler during a nocturnal test. The SiO cooler cooled to 13.8°C below ambient, while the blackbody cooler cooled to 13.4°C below ambient [2]. Therefore, a stronger cooler consists of silicon nitride (Si_3N_4), and the Al back reflector was fabricated in the following work [10]. Si_3N_4 has been explored again in a more recent work, showing a capability of sub-freezing temperature cooling (–22.2°C) [47]. The optical properties of silicon oxynitride (SiO_xN_y) have also been studied [55, 57], with its application as a selective cooler examined in [56]. As shown in Figure 4C [56], a 1.34-μm-thick $SiO_{0.6}N_{0.2}$ ($x=0.6$ and $y=0.2$) on the Al back reflector exhibits a strong emittance peak that matches the atmospheric window. The peak is related to the Si–O and Si–N bonds [67, 68] and the shoulder near 8.5 μm is related to the Si–H bond [67]. The net result was an equilibrium temperature of 16°C below ambient during nighttime, 2°C lower than what was achieved by a blackbody cooler [56]. For above-ambient cooling, it was found that fused silica is a suitable cooler with its high emittance across a broad wavelength range except for a dip within the atmospheric window. It is demonstrated to be able to cool an underlying Si wafer by 12°C [19]. Soda-lime glass or low-iron glass, commercially used as cover glass for PV, was found to be slightly better than fused silica for above-ambient cooling [69].

Radiative coolers in gaseous state have also been considered for radiative cooling applications. It is shown that for ammonia gas (NH_3), the IR absorption corresponding to the N atom moving perpendicularly to the H_3 plane is broadened by the rotational absorption so that it covers the atmospheric window [59]. Theoretical modeling showed that a slab of NH_3 gas can potentially cool down to 20°C below ambient during nighttime [59]. Similarly, with out-of-plane bending vibrations, ethylene (C_2H_4) also exhibits strong emittance in the atmospheric window, as shown in Figure 4D [58]. When encapsulated in an IR transparent container, C_2H_4 is a good candidate for radiative coolers that reached 10°C below-ambient cooling during daytime without direct sunlight [58]. Eriksson et al. showed that a mixture of C_2H_4 and C_2H_4O has higher cooling power, compared with either C_2H_4 or C_2H_4O [56].

3.2 Composite radiative coolers

As an alternative to bulk and gaseous material radiative coolers, composite material coolers consisting of two or more different materials were investigated, and were shown by several groups to have emittance properties suitable for radiative cooling. Commercially available white paints containing 35% TiO_2 provide a

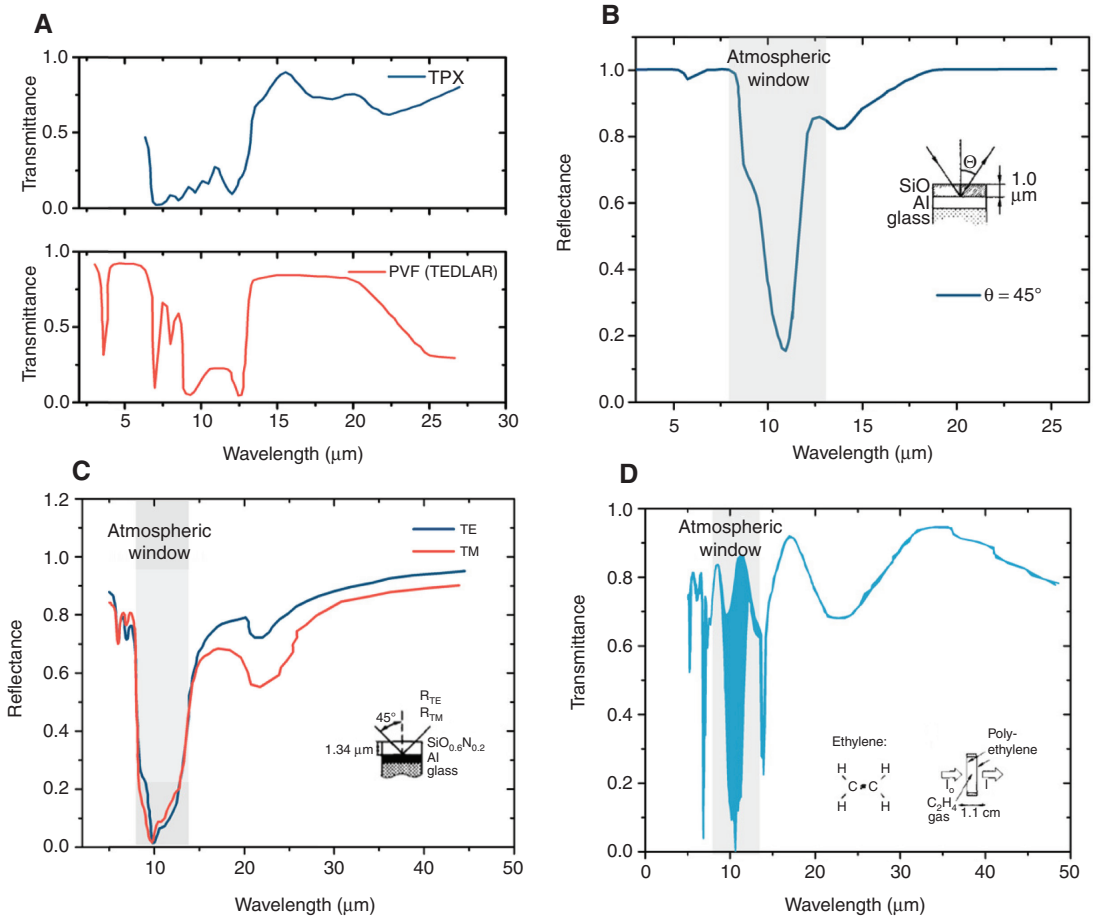

Figure 4: (A) Transmittance spectrum of aluminized polyvinyl fluoride (TEDLAR) cooler (red) and polymethylpentene (TPX) cooler (blue); adapted from [2, 52]. Strong emittance can be observed within the atmospheric window. (B) the measured reflectance spectrum of 10 μm SiO film on aluminum (Al). The spectrum is adapted from [2]. (C) The measured reflectance for TM (red) and TE (blue) polarizations incident on a 1.34 μm $SiO_{0.6}N_{0.2}$ film on Al. Compared to SiO, a broader peak is found within the atmospheric window. The spectrum is adapted from [56]. (D) The measured transmittance spectrum of ethylene gas in a 1.1-cm-thick gas slab. The spectrum is adapted from [58].

maximum 15°C drop in temperature with indirect sunlight, clear sky, and low absolute humidity; however, concerns regarding the true spectral selectivity of these TiO_2 paints were raised by Granqvist and Hjortsberg in their letter to the editor [70]. Additional experiments that applied white pigmented paints consisting of TiO_2/$BaSO_4$ or TiO_2/ZnS in alkyd resin binder on Al panels showed a 9–12°C temperature drop under nocturnal conditions [8].

The development of nanomaterials offered more choices of cooler design. Suryawanshi and Lin fabricated and tested three types of above-ambient radiative coolers consisting of carbon-based nanomaterials [nanodiamond powder (NDP), multi-wall carbon nanotubes (CNTs), or carbon black (CB)] dispersed in acrylate (AC) emulsion with the Al back panel [60]. It was found that the composite cooler with a CNT gives the best performance among the three, as shown in Figure 5A. Furthermore, 1 wt% of CNT in AC can lower the temperature by 17°C from 87°C [60]. Similarly, nanoparticles that have absorption bands that match the atmospheric window were added to polymeric binders to form radiative coolers for below-ambient cooling. It was found that the two IR absorption bands of SiO_2 and SiC nanoparticles, as shown in Figure 5B, are complementary to each other. Therefore, when the two nanoparticles are mixed together in the polyethylene film, the emittance spectrum matches well with the atmospheric window [61]. The estimated result from the model proposed in [61] showed that a 25°C temperature drop below ambient can be achieved when there are limited non-radiative heat transfer and no sunlight. Other than polyethylene, PVF and polyvinylidene fluoride are also good polymeric binders for SiO_2 and SiC nanoparticle composite radiative coolers [71].

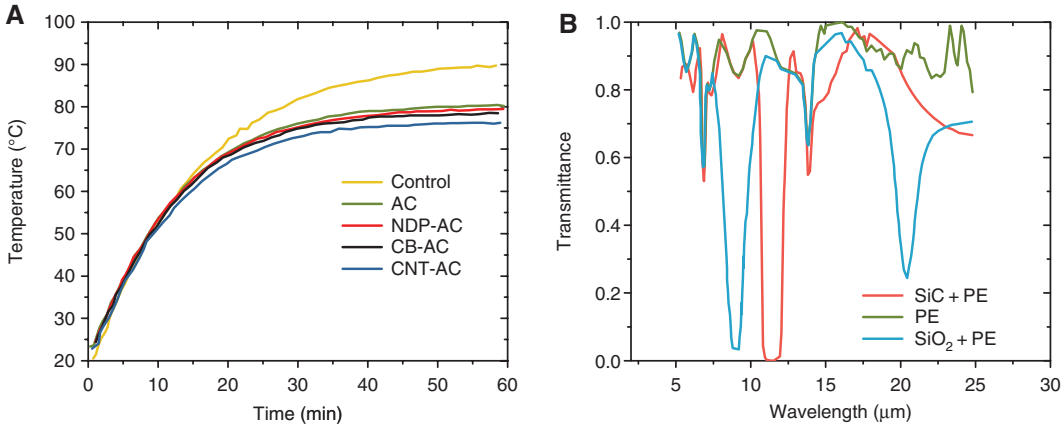

Figure 5: (A) Operating temperature vs. time for carbon-based nanomaterial-composite coolers. The cooler with multiwall carbon nanotubes (CNT-AC) gives the best performance. Adapted with permission from [60]. Copyright (2009) American Chemical Society. (B) The transmittance spectrum of SiO_2 nanoparticles in polyethylene binder (blue) and SiC nanoparticles in polyethylene binder (red). The transmittance spectrum of the polyethylene film itself [61] is shown in green. The two nanoparticle emission peaks are complementary to each other, and both fit within the atmospheric transparency window.

3.3 Nanophotonic radiative coolers

Nanophotonics opens up new possibilities to tailor the emittance spectrum via properly designing periodic nano/micro-structures, in analogy with prior efforts in photovoltaics [72] and TPV [73, 74]. Similarly, for radiative cooling, the large degree of freedom in engineering nanophotonic structures potentially allows for better cooling performance than bulk material or composite coolers. It is proposed that a bar array consisting of α-quartz gives strong selective thermal emission within the atmospheric window while preserving the solar absorption of the underlying structure (Si nanowire array on Al) [63]. The simulation showed that the temperature drop during daytime can be as large as 31.4°C with a nonradiative heat exchange coefficient equal to 6 W/(K m^2) [63]. Stronger selectivity in thermal emittance can be achieved by more complex PhC structures. Raphaeli et al. proposed a structure consisting of two layers of quartz and SiC 2D PhC on top of a 1D chirped dielectric stack and silver (Ag) substrate [16]. As shown in Figure 6A, the structure proposed has a strong emittance spectrum that matches well with the atmospheric window due to the phonon-polariton resonances of quartz and SiC. Meanwhile, the introduction of a chirped dielectric reflector and the intrinsically low solar absorption of both quartz and SiC strongly suppressed solar absorption so that below-ambient cooling can be achieved during daytime [16]. The simulation showed that with the optimized PhC structure, a temperature of 7°C below ambient can be reached with a non-radiative heat exchange coefficient of 12 W/(K m^2) [16]. In experimental demonstrations, it was shown that a much simpler nanophotonic cooler structure also cools to 4.9°C below ambient under direct sunlight [17]. Figure 6B shows the emittance spectrum of the fabricated radiative cooler. The SEM cross-section of the cooler which consists of seven alternating layers of SiO_2 and HfO_2 on top of Ag is shown in the inset [17]. The significance of the result is that a properly designed one-dimensional photonic film that is feasible for large-scale fabrication could achieve below-ambient cooling in daytime. However, a low-density polyethylene film, serving as a convection barrier, is used in the experiment. The non-radiative heat transfer was therefore strongly suppressed, giving more significant below-ambient cooling effect. Fortunately, such below-ambient cooling in daytime can be achieved even without convection barriers [66]. Using multilayer polyester stacks, Gentle and Smith demonstrated 2°C below-ambient cooling under mid-summer sunlight without using convective barriers [66].

For above-ambient cooling during daytime, nanophotonic coolers also showed promising performance. It was proposed by Zhu et al. [18] that a 2D square lattice of SiO_2 pyramids can reduce the temperature of the underlying Si solar cell by 17.6°C. Later, their experiments demonstrated that a 2D PhC consisting of a square lattice of air holes on SiO_2 cools the underlying Si wafer by 13°C [19]. Figure 6C shows the emittance spectrum of the SiO_2 PhC and its top-view SEM cross-section in the inset. Apparently, the PhC structure enhances the thermal emittance of bare SiO_2 within the atmospheric window, yielding an equilibrium temperature that is 1°C lower than the case with bare SiO_2 [19]. A similar 2D PhC structure can enhance the thermal emittance of low-iron soda-lime glass as well. It is shown in Figure 6D that a square lattice of air holes on low-iron

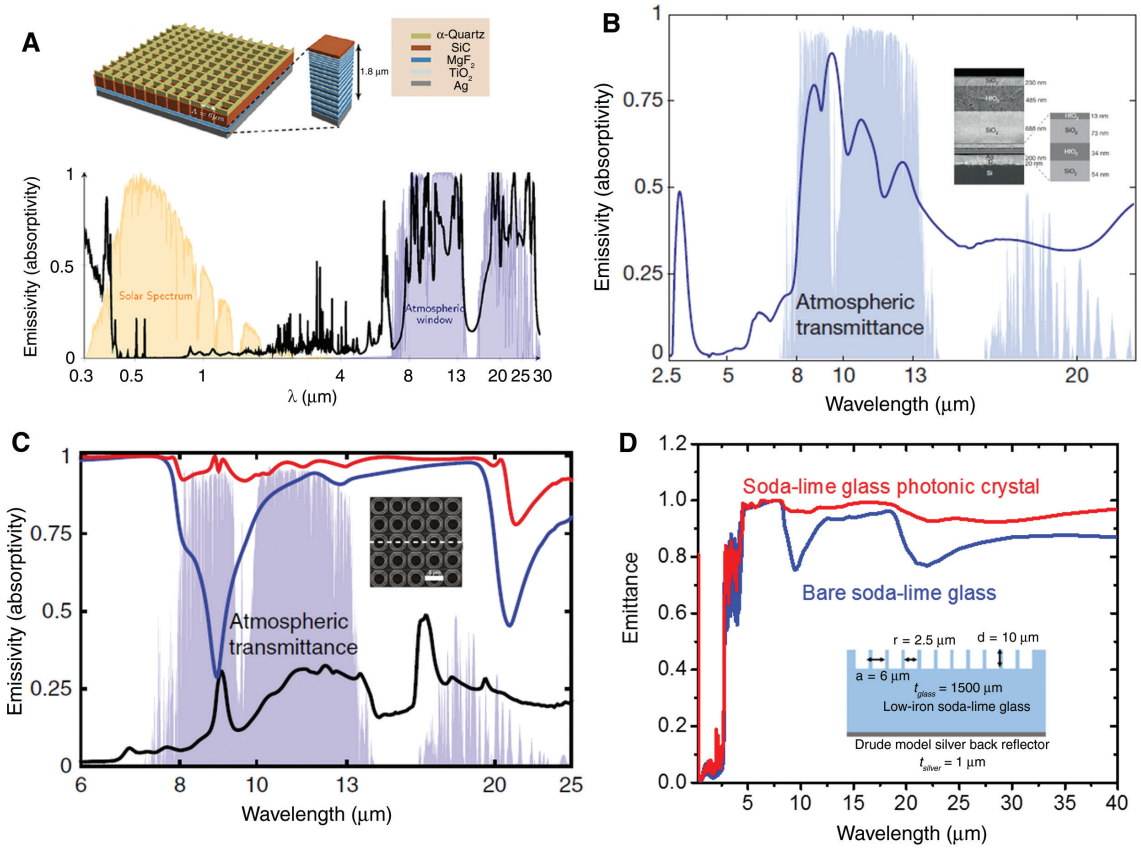

Figure 6: (A) The numerically optimized photonic crystal cooler for a below-ambient cooler under direct solar exposure. Reprinted with permission from [16]. Copyright (2013) American Chemical Society. (B) The measured emittance spectrum of the fabricated 1D photonic crystal cooler with feasible structures and excellent emittance within the atmospheric window. Adapted with permission from Macmillan Publishers Ltd (Nature) [17], copyright (2014). (C) The measured emittance spectrum of a bare silicon wafer (black), a bare silica slab (blue) and a 2D photonic crystal of silica (red). It can be seen that the emission of silica in the atmospheric transparency window can be enhanced by the 2D square lattice structure. The figure is adapted from [19]. (D) Simulated emittance spectrum of bare low-iron soda-lime glass (blue) and 2D photonic crystal-enhanced bare low-iron soda-lime glass (red). A similar effect of enhanced emission within the atmospheric window is observed. The broad emission spectrum and low solar absorption is ideal for above-ambient daytime cooling. The figure is adapted from [64].

soda-lime glass (structure cross-section in the inset) provides an almost uniform emittance that is close to unity in mid-IR and is highly reflective in the solar spectrum, which is close to the ideal case for above-ambient radiative cooling during daytime [64]. Simulations showed that such radiative cooler design cools a photovoltaic diode of a specific energy conversion device with high heat load, known as TPV, by 91°C from 161°C, which will be discussed in detail in Section 4. The amount of cooling can significantly increase the efficiency of the TPV system and improve the reliability thereof.

3.4 Summary

Various radiative coolers can be quantitatively compared by the cooling parameters defined in a way similar to [2]. From the discussion in Section 2, radiative coolers for below-ambient or above-ambient cooling have different ideal emittance spectra. Therefore, a pair of cooling parameters should be defined to capture the different requirements. Following the work by Granqvist et al. [2], the spectrally averaged hemispherical emittance inside the atmospheric window $\varepsilon_{\text{ave–in}}$ is defined as

$$\varepsilon_{\text{ave–in}} = \frac{\int_{8\,\mu\text{m}}^{13\,\mu\text{m}} d\lambda\, I_{BB}(\lambda, T_a)\varepsilon(\lambda)}{\int_{8\,\mu\text{m}}^{13\,\mu\text{m}} d\lambda\, I_{BB}(\lambda, T_a)}, \tag{6}$$

where $\varepsilon(\lambda) = \int_0^{\pi/2} d(\sin^2\theta)\varepsilon(\lambda, \theta)$ and $I_{BB}(\lambda, T)$ is Planck's blackbody radiation function from Eq. (1). The spectrally

averaged hemispherical emittance outside the atmospheric window $\varepsilon_{ave-out}$ is defined as

$$\varepsilon_{ave-out} = \frac{\int_0^\infty d\lambda\, I_{BB}(\lambda, T_a)\varepsilon(\lambda, T_a) - \int_{8\,\mu m}^{13\,\mu m} d\lambda\, I_{BB}(\lambda, T_a)\varepsilon(\lambda)}{\int_0^\infty d\lambda\, I_{BB}(\lambda, T_a) - \int_{8\,\mu m}^{13\,\mu m} d\lambda\, I_{BB}(\lambda, T_a)}. \quad (7)$$

It should be noted that this term is different from the spectrally averaged hemispherical emittance over the entire spectrum ε_{ave} defined by Granqvist et al. But it can be derived from ε_{ave} by substituting the first term in the numerator of Eq. (7) with $\varepsilon_{ave}\int_0^\infty d\lambda\, I_{BB}(\lambda, T_a)$. One important reason of picking these two parameters, as pointed out by Granqvist et al. [2], is that they do not depend strongly on the operating temperature of the cooler and can be easily used to estimate the cooling power at certain temperatures. For some of the radiative coolers discussed above, their cooling parameters are mapped in Figure 7. For the coolers labeled with *, the cooling parameters are calculated based on published spectra and are limited by the spectral range presented. The top-left corner of the plot (blue shaded region) corresponds to the ideal emittance profile of a cooler for below-ambient cooling, while the top-right corner (red shaded region) corresponds to the ideal emittance profile of an above-ambient cooler. It is apparent that most demonstrated and proposed coolers lie in the top-left corner, and are therefore more suitable for below-ambient cooling. However, two designs (silica PhC (2015) [19] and PhC (2016) [64]) lie in the top-right corner, and are both strong candidates for above-ambient cooling. The map shows that bulk material coolers such as $SiO_{0.6}N_{0.2}$ and Si_3N_4 and gaseous coolers such as C_2H_4 and NH_3 already have good emittance spectra that are suitable for below-ambient cooling. Besides, although the absolute cooling of PhC designs is not always as good as bulk material coolers developed much earlier, their solar absorption can be suppressed much more significantly. This is an unprecedented advantage that enables below-ambient cooling even under direct sunlight. Remarkably, the map shown in Figure 7 clearly differentiates the performance of different coolers for both above-ambient and below-ambient cooling. It also allows a quantitative comparison between different cooler designs, as well as estimating their cooling power. In the next section, we consider how various materials and designs can be applied to specific applications.

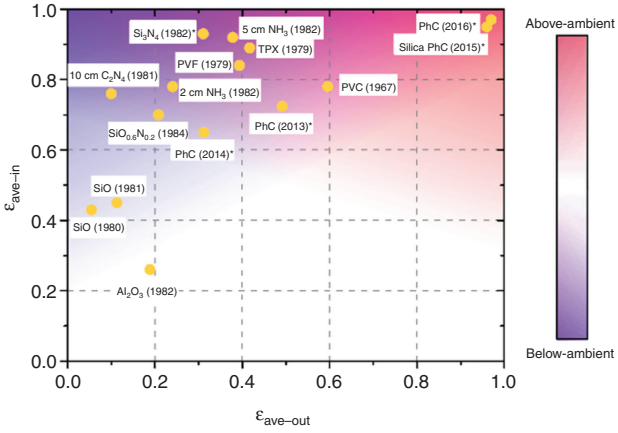

Figure 7: Cooling parameters of selective radiative coolers. The top-left corner (blue shaded region) implies the best below-ambient cooling performance. The top-right corner (red shaded region) implies the best above-ambient cooling performance. Data points with * were calculated by the author, using detailed spectra previously presented in the references. Reference list: PVC (1967) [5], TPX (1979) [2], PVF (1979) [2], SiO (1980) [11], SiO (1981) [2], 10 cm C_2H_4 (1981) [58], Al_2O_3 (1982) [75], Si_3N_4 (1982)* [10], 2 cm NH_3 (1982) [59], 5 cm NH_3 (1982) [59], $SiO_{0.6}N_{0.2}$ (1984) [56], PhC (2013)* [16], PhC (2014)* [17], Silica PhC (2015)* [19], PhC (2016)* [64].

4 Cooling system applications

The preceding section has provided a comprehensive overview of the various designs of radiative coolers. In this section, we will examine the corresponding system-level applications enabled by radiative cooling. First, using radiative cooling to improve the performance and reliability of conventional (one-sun) solar modules by lowering operating temperature has recently drawn a great deal of attention [18–22, 69]. Here, we will discuss the radiative cooling of solar modules from both the theoretical and experimental perspectives. Radiative cooling is also of great interest to systems with serious self-heating issues, such as CPV and TPV due to the possible cost reduction by eliminating active cooling. Recent studies of applying radiative cooling to CPV and TPV will be discussed [48, 64]. Second, a novel emissive energy harvesting (EEH) system has been proposed to harness nighttime radiative cooling power for power generation. We will discuss the fundamental limit of the power output of EEHs and the prospect of adopting long-wave IR rectennas and cold carrier absorbers for these applications [49, 76]. Finally, the potential benefits of radiative cooling for IR detectors and electronics will be discussed.

4.1 PV cooling

PV, especially solar PV, is an alternative energy source that has the potential to reduce our dependence on fossil fuels

for the 21st century. A typical commercial solar module has an efficiency of 20%, which means that up to 80% of solar irradiance is dissipated as heat, thereby increasing the module temperature. On average, one-sun solar modules can operate 20–40°C higher than the ambient temperature. Self-heating becomes even worse for CPV as well as TPV since the incoming light can be orders of magnitude higher than that of one-sun solar modules. For the short term, the elevated temperature directly reduces the power conversion efficiency of PV cells, for example, temperature coefficient of −0.45%/°C for crystalline silicon. In the long run, the aging rate for solar modules can double with every 10°C increase in average temperature [77], caused by thermally activated degradation processes, such as corrosion and potential-induced degradation [78, 79]. Hence, cooling photovoltaic cells can dramatically improve performance and reliability, leading to greater energy yield.

4.1.1 One-sun solar PV

Low IR emissivity can exacerbate self-heating in PV [18–22, 69]. As shown in Figure 4 in [22], the emittance of bare silicon in the IR spectrum is very low; therefore, it emits negligible thermal radiation. Indeed, bare silicon cells can operate up to 20°C higher than glass-encapsulated modules [18, 19, 22], which has much higher emittance. Nonetheless, its emittance still drops significantly within the atmospheric window, preventing heat exchange with the cold universe. Additionally, the emittance of glass decreases rapidly at an angle of incidence θ greater than 50°, further suppressing thermal radiation (see Figure 4 of [22]). Note that the rear side of the solar modules also exchanges thermal radiation with the ground. During the day, the ground underneath the solar modules can be at a lower temperature than the ambient owing to shading, potentially providing considerable cooling power. The PVF backsheet (an encapsulant polymer) has a hemispherical emittance, $\varepsilon_{ave} \approx 0.85$, still lower than the unity. As a result, there is still room to improve the radiative cooling of the top (glass) and bottom (PVF backsheet) layers of solar modules. This brings about a question of the maximum temperature reduction achievable by radiative cooling for a one-sun solar module. Reference [18] shows a temperature difference of 5.2°C between fused-silica glass ($\varepsilon_{ave} \approx 0.73$) and ideal radiative cooler ($\varepsilon_{ave} = 1$) as the top layer for solar panels. The cover glass of commercial solar modules, however, has higher hemispherical emittance ~0.84 than fused-silica glass; thereby the actual cooling gain may have been overestimated in [18]. Indeed, simulation results in [22, 69] predict a temperature reduction of only 1–2°C by radiative cooling when commercial glass is considered (see Figure 8). Zhu et al. [19] experimentally demonstrated radiative cooling on solar cells by using a PhC emitter as the top layer (its emittance is plotted in Figure 6C). Figure 9A illustrates the experimental setup, and the steady-state temperature of the solar absorber with the PhC emitter was measured to be $\sim\Delta T \approx 1.3$°C cooler than that of fused silica in [19] (ΔT is expected to be slightly lower for PhC vs. commercial cover glass) (see Figure 9B). Even such a modest temperature change can yield an ~0.13% absolute increase in efficiency for Si solar modules. Given the efficiency plateau of Si-based PV in the recent decade [80], radiative cooling gives a new perspective for further improving the efficiency of Si solar modules. Moreover, the time to failure of solar modules follows the Arrhenius relation (i.e. it is proportional to $\exp(-E_A/kT)$, where $E_A \approx 0.89$ eV is the activation energy [81]). Radiatively cooling the solar module by 1–2°C can extend lifetime by up to 20%, substantially increasing the lifetime electricity yield. Hence, radiative cooling can improve the performance and reliability of one-sun solar modules considerably.

4.1.2 CPV and TPV

Radiative cooling is of great interest to systems that are under excessive heat dissipation and require energy-efficient and

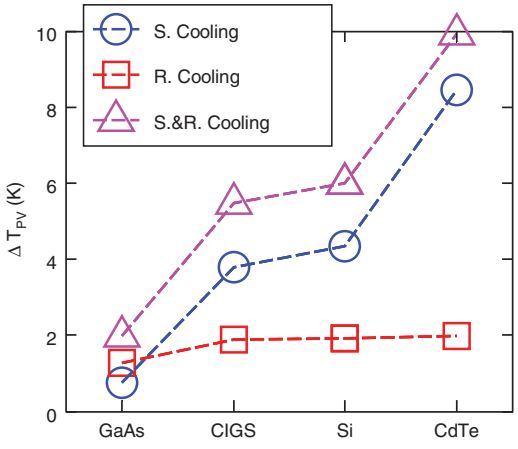

Figure 8: Simulated temperature reduction obtained by different cooling schemes (S. Cooling: selective-spectral cooling; R. Cooing: radiative cooling; S.&R. Cooling: selective-spectral cooling and radiative cooling combined). The simulation assumes that the wind speed is approximately 0.5 m/s giving an effective convective coefficient $h = 10$ W/(K m^2), conductive heat transfer only at the module edges through metal frames is neglected, and the ambient temperature T_A and solar irradiance are 300 K and 1000 W/m^2, respectively. The atmospheric transmittance data are for New Delhi in spring, with perceptible water vapor (PWV) = 18 mm. © 2017 IEEE. Reprinted, with permission, from [22].

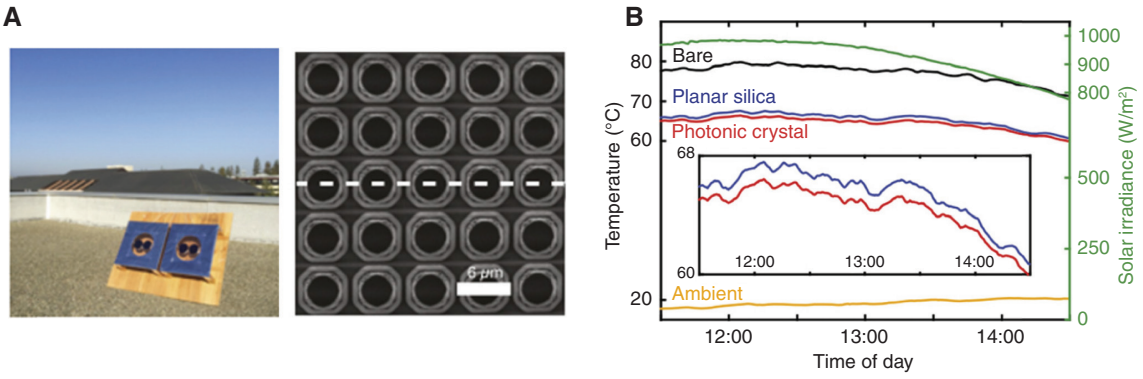

Figure 9: (A) Experimental setup for radiative cooling in [19]. The left picture shows the apparatus and solar absorbers on a rooftop. The chambers were tilted at 60° to maximize solar absorption. Shown on the right is the normal view SEM image of the 2D silica photonic crystal structure (PhC) consisting of a square lattice PhC of 10 μm deep air holes with a periodicity of 6 μm fabricated on a fused silica wafer. (B) Temperature measurement of solar absorbers underneath different top layers on a clear day in winter. The measurement was performed with a windshield to reduce the convection coefficient to 6.5–9.1 W/(K m²).

effective cooling schemes. In this context, radiative cooling appears particularly appealing to CPV and TPV systems.

CPV, an extension of one-sun PV, operates under concentrated sunlight (up to 100-fold), resulting in severe self-heating. Despite the use of traditional passive cooling, the operating temperature of CPV under 24 suns can still reach up to 140°C [82], considerably lowering the power output as well as shortening the lifespan. So far, most work on cooling techniques for CPV has been limited to heat sinks [83], cycling coolants [84], and forced air cooling [85], all of which can add up the cost of CPV systems and reduce the overall energy efficiency. Recently, by coating the bottom aluminum chassis with an additional thermal radiation layer to enhance thermal radiation, Nishioka et al. [48] successfully achieved temperature reduction by 10°C corresponding to 1% absolute improvement in efficiency for triple-junction CPV systems under 820 concentration factor (see Figure 10). Note that the enhanced thermal radiation in [48] is purely from improved heat exchange with the ground. Extra cooling gain can be obtained by reconfiguring the CPV system to direct the enhanced thermal radiation toward the sky, whose temperature is much lower than the ground.

Likewise, TPV can also experience radiative heat stress on the order of hundreds of suns in vacuum (to thermally isolate the thermal emitter), resulting in a severe thermal management challenge. The temperature of TPV systems with only passive cooling can easily go beyond 200°C, and the consequent efficiency drop can be over 50% [23]. Zhou et al. [64] proposed a setup for radiatively cool outdoor TPV applications. The setup consists of a cooling radiator on top of a heat spreader to thermally concentrate the radiative cooling power on the PV cells underneath. Using an opto-electro-thermal coupled simulation framework, a temperature drop of 90°C of TPV cells by radiative cooling has been predicted in [64] (see Figure 11A). With sufficient cooling concentration factor (area ratio between the radiative cooling emitter and the

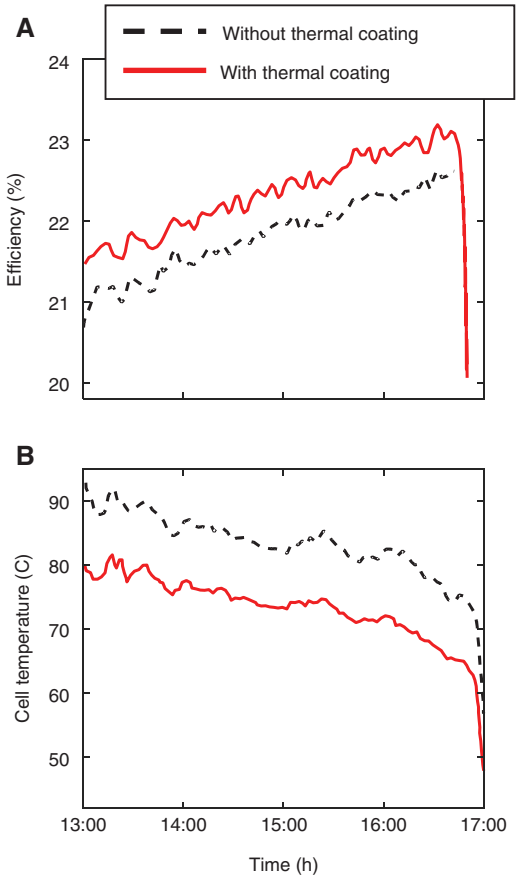

Figure 10: The recorded (A) operating temperature and (B) efficiency of triple-junction concentration photovoltaic systems under 820 suns concentration with and without thermal radiation coating in [48].

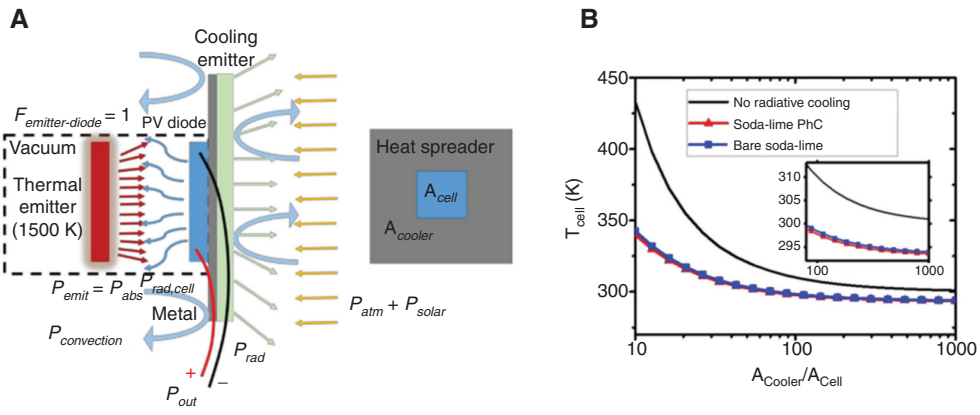

Figure 11: (A) The design of an outdoor TPV system with radiative cooling. The thermal emitter and PV cell are both enclosed in a vacuum for mutual thermal isolation. The area of the radiative cooler and heat spreader is larger than that of the PV cell to improve cooling power. (B) Operating temperature of PV cell as a function of the cooler-to-cell area ratio. The convection coefficient is set to be 2.5 W/(K m^2).

PV cell), below-ambient cooling of TPV during daytime can be realized by employing low-iron soda-lime glass as the radiative cooler, allowing TPV exceeding the optimal efficiency at room temperature (see Figure 11B). The design of radiative cooling in [64] is also transferable to indoor TPV, though the indoor background temperature bounds the lowest achievable cooling temperature.

4.1.3 Discussion

Though radiative cooling can improve the short-term efficiency and long-term reliability for one-sun PV, CPV, and TPV, one still needs to consider the viability and cost in practice. For example, fabricating PhC for radiative cooling can be very expensive and not suitable for large-scale applications. The deep air holes in PhC could increase susceptibility to soil accumulation, especially in dry environments. On the other hand, selective-spectral cooling for photovoltaic applications, that is, preventing sub-bandgap heating by reflecting the near-IR solar spectrum, has been proposed in [22]. As shown in Figure 8, the cooling gain of selective-spectral cooling can be superior to radiative cooling for most of the terrestrial solar modules of different technologies; for example, selective-spectral cooling and radiative cooling reduce the temperature of one-sun CdTe solar modules by ~8°C and ~2°C, respectively. Hence, selective-spectral cooling can be more advantageous for one-sun terrestrial solar modules, unless inexpensive highly IR emissive cover materials are developed. Nonetheless, for systems with much greater heat load (e.g. CPV and TPV) as well as extraterrestrial PV (no air convection), radiative cooling remains a promising research opportunity for future study.

4.2 Emissive energy harvester

The earth is constantly radiating approximately 10^{17} W to the cold universe [49]. In principle, if properly utilized, radiation from the earth is sufficient to meet the electricity need for the entire humanity. However, effective strategies to harness such energy have not been fully explored. Recently, a device named emissive energy harvester (EEH) that can transfer heat from a heat sink to sky through radiative cooling from a cold reservoir and convert part of the heat flow into useful work has been proposed [49, 76] (see Figure 12A). Coupled Carnot's law to the steady-state heat flow, the maximum output power from the engine is $P_{Cool} \times (T_{Hot}/T_{Cold} - 1)$, where P_{Cool} is the net radiative cooling power from the cold reservoir to the sky described by Eq. (4). At a fixed T_{Hot} and T_{Sky}, P_{Cool} increases with T_{Cold} whereas the Carnot efficiency of the engine decreases. Hence, there is an optimal temperature of the cold reservoir that maximizes the power at a given T_{Hot} and T_{Sky}. Figure 12B–C summarizes the performance of an ideal EEH (Carnot limited) with different emission bandwidths [76]. The power density can reach up to ~300 W/m^2 (equivalent to a solar cell with 30% efficiency under one sun) with heat sink at a temperature of 500 K. It should be noted that, at high heat sink temperature that gives an optimal T_{Cold} above the ambient, it is not desirable to confine the wavelength range of thermal radiation within the atmospheric window because of the additional outgoing heat from the colder reservoir to the surrounding background.

Ideally, in analogy to PV, EEHs can be realized by a semiconductor p-n junction. However, dominant Auger recombination and generation in mid-IR bandgap semiconductors makes such a design impractical. As shown

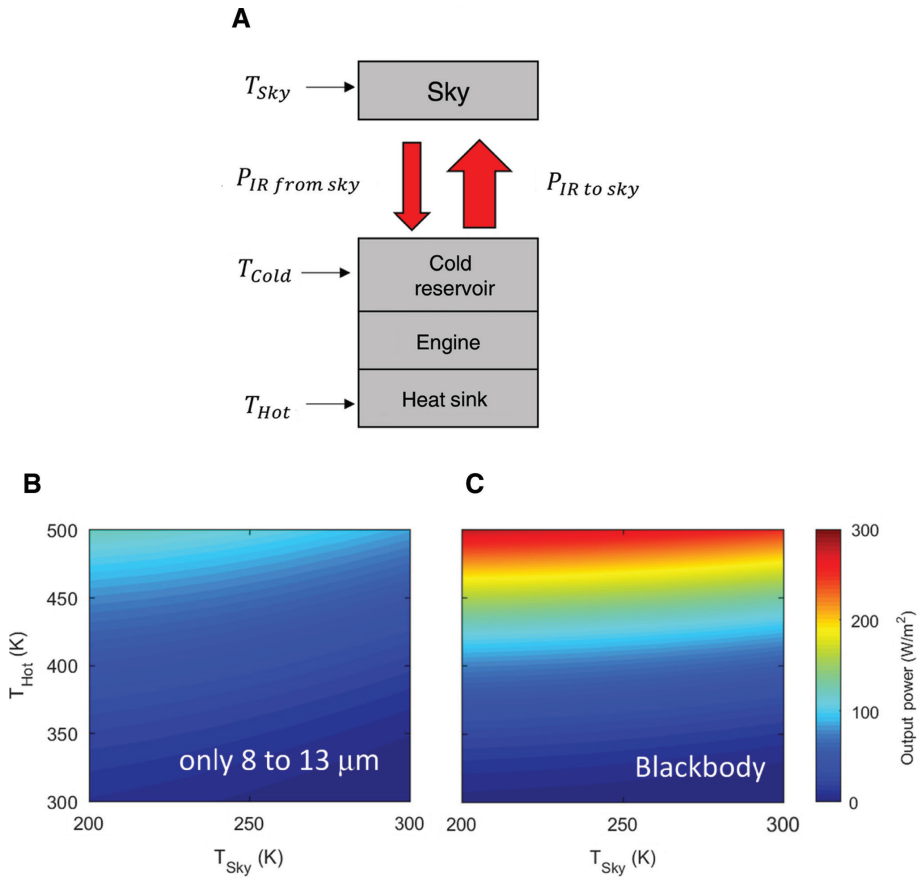

Figure 12: (A) Schematic of an EEH. Heat flows from the heat sink to the cold reservoir through the engine, which converts part of the heat into useable energy; the rest of the heat is radiated to the sky by the cold reservoir (or to the surroundings with non-zero emissivity outside the atmospheric window). Carnot-limited output power (W/m^2) of an ideal EEH that (B) only emits between 8 and 13 µm wavelengths with a unity emissivity and (C) emits as a blackbody upwards placed outdoor at an ambient temperature of 300 K.

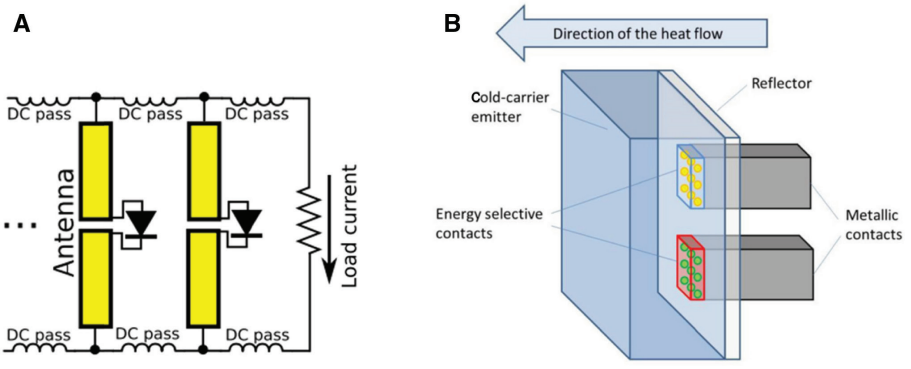

Figure 13: (A) Design of a rectenna-based EEH, where the electrical signal is coupled to IR radiation collected by antennas. (B) Illustration of a cold carrier EEH. Electrical current is extracted by energy-selective metallic contacts. The back reflector is used to reduce radiative heat transfer between the cold electrons and the heat source. Reproduced from [76], with the permission of AIP Publishing.

in Figure 13, much more promising candidates have been proposed, that is, rectenna-based and cold carrier EEHs [49, 76], both of which will be discussed in detail as follows.

4.2.1 Rectenna-based EEH

Traditionally, a rectenna is a rectifying antenna that can create DC current from electromagnetic microwaves.

Recently, rectenna-based applications for high-frequency radiation up to the visible spectrum have been demonstrated [86–90], which inspires the implementation of EEHs using rectennas. As pointed out in [49], there are two potential challenges for realizing rectenna-based EEH, namely, IR antennas and low-voltage diode asymmetry. Given the recent development of high-frequency antennas, the first (IR antenna) is relatively straightforward. Recent advances in soft lithography can even allow cost-friendly manufacture of large-area IR antennas [91]. The latter (low-voltage diode asymmetry), however, appears to be much more challenging. For instance, the oscillating thermal noise voltage across the diode is expected to be ~1 mV_{rms} for the IR rectenna in [92]. At such low voltage, the diode has insufficient asymmetry and essentially acts as a resistor, preventing DC power generation from the rectenna circuit. Two solutions to resolve inadequate diode asymmetry have been proposed in [49]. First, use a high-voltage rectenna by matching a high-impedance antenna to a high impedance diode or a broadband impedance transformer to compensate the impedance difference. Recent progress on the terahertz transmission line [93] with high impedance as well as plasmonic waveguides with the three-dimensional taper line [94] can shed some light on the future development of impedance transformers with wide bandwidth, though they are not available yet. Second, diodes with a high ratio of forward-backward conductance at low voltage, for example, tunneling and ballistic diodes, can also provide sufficient diode asymmetry for rectenna-based EEHs. Though rectenna-based EEHs show great promise for further exploration, it is not the only possibility for EEHs. Next, we will review another design, namely, cold carrier EEHs.

4.2.2 Cold carrier EEH

Cold carrier EEHs have a similar device configuration compared to hot carrier solar cells but operates in the completely opposite manner [76]. The working principle of hot carrier solar cells is to reduce thermalization loss by suppress carrier cooling (phonon absorption) and extract those hot carriers through narrow energy bands or discrete states by selective contacts [95]. In cold carrier EEHs, however, decoupling carriers and phonons is not to prevent carrier cooling but rather carrier heating. By a net photon flux from the EEH emitter to the sky and surrounding, the electron temperature is reduced. The redistribution of electron in the emitter due to colder temperature (at T_{Cold}) triggers electron transport from the selective contacts (at T_{Hot}) within a narrow bandwidth or at discrete states, therefore generating DC electric power (see Figure 13B). Note that the efficiency of cold carrier EEHs increases with the smaller bandgap of the emitter because of greater net radiation to the surroundings. It, however, comes with a penalty; specifically, inevitable non-radiative mechanisms at low bandgap such as impact ionization and Auger recombination can reduce the quasi-Fermi level splitting and consequently open-circuit voltage [96]. Recently, Santhanam and Fan have experimentally demonstrated cold-carrier EEHs using a negatively illuminated photodiode made of HgCdZnTe with a bandgap of 218 meV [97]. The extracted power density normalized to the effective optical area of the diode (0.1 mm^2), however, is only on the order of 10^{-5} W/m^2 far below the Carnot-limit because of non-ideality such as nonradiative recombination, finite carrier mobility, and finite contact resistance. Simulation in [97] has suggested that, by reducing nonradiative recombination and contact resistance, one can substantially improve the output power up to ~10 W/m^2 with exposure to the 3 K cosmic background. It has also been suggested in [97] that switching material systems to III–V semiconductor compounds with dilute concentrations of nitrogen can further increase the power density of cold carrier EEHs by suppressing Auger recombination.

4.2.3 Discussion

Beyond the mentioned EEH implementation hereof, other strategies include using thermoelectric devices as well as multi-quantum-well heterostructures [49] to harness energy via radiative cooling. As suggested in [49, 98], the output power of EEHs can be even improved by up to five and ten times through solar heating and thermal extraction, respectively. Even though the practical use of EEHs still requires additional work and experimental demonstration, in principle, it already shows certain advantages over conventional renewable energy sources. For instance, one of the biggest challenges of conventional renewable energy is intermittent availability, for example, there is no sunlight at night for PV and wind power may not be accessible for certain seasons. Such high temporal fluctuation of power can induce considerable stress on the grid system and requires an additional storage system for continuous electricity supply. On the other hand, radiative cooling is incessant, so is the energy yield. Thus, EEHs do not have the issue of intermittence. Beyond terrestrial energy harvesting, EEHs can also be a very promising candidate for space applications. A space vessel at 300 K covered by EHHs can siphon power up to 50 W/m^2 by exchanging radiative energy with the 3 K cosmic background [76], and even to 90 W/m^2 at 350 K. Despite the great potential

of EEHs, whether they can play an important role in the renewable energy landscape remains an interesting open question until further research efforts have been made.

4.3 IR detectors and electronics

4.3.1 IR detector

An IR detector is essentially a transducer that converts radiative energy in the IR spectrum to measurable signals. IR detectors have already been used in a wide range of applications, including rail safety, gas leak detection, flame detection, temperature sensing, etc. Primarily, IR detectors can be categorized as either optoelectronic (quantum) detectors or thermal detectors (e.g. pyroelectrical, thermoelectric, thermos-resistive). To achieve very high responsivity as well as detectivity (two most important figures of merit for IR detectors), most of the optoelectronic IR detectors require *cryogenic* operation even down to 77 K (liquid nitrogen) [99] to suppress thermal generation of carrier and thermal noise so as to improve quantum efficiency [100]. Thermal IR detectors, on the other hand, can still function near room temperature. The response time of uncooled thermal IR detectors, however, can be very slow ($>10^{-3}$ s) due to the fluctuations of the background temperature [101]. Thus, radiative cooling can be of great interest to IR detectors, particularly for those located outdoors, or at places where deploying active cooling can be difficult. When the target temperature of radiative cooling is below the surrounding temperature, great caution should be taken to reduce any non-radiative heat transfers (e.g. convection and conduction) from the surroundings to the detectors. Though radiative cooling appears to enhance the responsivity and detectivitiy, there has not been any research progress on this topic to the best of our knowledge. We hope that this paper can motivate the prospect of radiative cooling on IR detectors and spur more research efforts.

4.3.2 Electronics

In the direction toward much smaller yet more powerful electronics, the power density of modern electronics has increased, dramatically raising serious concerns on self-heating [102–105]. In large systems (e.g. computer clusters), one of the challenges is maintaining all transistors within the specified operating temperature range. Experiments have indicated that the temperature of working transistors can reach up to 50°C higher than the room temperature [106]. Note that most of the degradation mechanisms in electronics such as negative-bias temperature instability [107] or electromigration [108] depend on temperature exponentially. Thereby, a 10–15°C increase in temperature can halve the lifetime of microprocessors [109]. For small systems like handheld devices, it is crucial to maintain the surface temperature below a certain threshold (45 and 41°C for plastic and aluminum enclosure, respectively [110]), so it does not cause any discomfort to the users. For small portable devices running on batteries, however, passive cooling is preferred to maximize battery life. It has been shown that over half the heat dissipation in a tablet can be via radiation [111], and the internal temperature difference in electronics attributed to radiation can be more than 12°C [112]. Despite the importance of radiative cooling, it has been mostly overlooked in the electronics industry [113]; however, given the promising potential of radiative cooling for severely self-heated modern electronics, we encourage researchers to investigate the viability and implementation of this subject further.

5 Conclusions

In conclusion, we have demonstrated that the basic principles of radiative cooling allow for substantial rates of passive cooling via exchange of long-wavelength IR radiation with the sky above. Below-ambient cooling is enabled by the atmospheric window, ranging from approximately 8–13 μm. A combination of careful materials choice and nanophotonic design is the key to maximizing the potential of radiative cooling. Done properly, this approach should enable a broad range of applications, which include temperature-sensitive opto-electronic devices, such as PV, TPV, rectennas, IR detectors, and electronics. Nonetheless, a number of challenges remain for future research, which include demonstrating solar-blind below-ambient cooling, demonstrating increased efficiency in energy conversion applications, and demonstrating a scalable process for low-cost production.

Acknowledgments: We thank Mohammad Ryyan Khan for valuable discussions. Support was provided by the Department of Energy, under DOE Cooperative Agreement No. DE-EE0004946 (PVMI Bay Area PV Consortium),

and the National Science Foundation Award EEC 1454315 – CAREER: Thermophotonics for Efficient Harvesting of Waste Heat as Electricity, and the NCN-NEEDS program under Contract 1227020-EEC, and by the Semiconductor Research Corporation.

References

[1] Catalanotti S, Cuomo V, Piro G, Ruggi D, Silvestrini V, Troise G. The radiative cooling of selective surfaces. Sol Energy 1975;17:83–9.
[2] Granqvist CGC, Hjortsbery A, Hjortsberg A. Radiative cooling to low temperatures: general considerations and application to selectively emitting SiO films. J Appl Phys 1981;52:4205.
[3] Craig R. The upper atmosphere: meteorology and physics. New York, Academic Press, 1965.
[4] Bahadori MN. Passive cooling systems in Iranian architecture. Sci Am 1978;238:144–54.
[5] Trombe F. Perspectives sur l'utilisation des rayonnements solaires et terrestres dans certaines régions du monde. Rev Gen Therm 1967;6:1285.
[6] Bartoli B, Catalanotti S, Coluzzi B, Cuomo V, Silvestrini V, Troise G. Nocturnal and diurnal performances of selective radiators. Appl Energy 1977;3:267–86.
[7] Nilsson T, Niklasson GA, Granqvist C. A solar-reflecting material for radiative cooling applications: ZnS pigmented polyethylene. Sol Energy Mater Sol Cells 1992;28:175–93.
[8] Orel B, Gunde M, Krainer A. Radiative cooling efficiency of white pigmented paints. Sol Energy 1993;50:477–82.
[9] Nilsson TMJ, Niklasson GA. Radiative cooling during the day: simulations and experiments on pigmented polyethylene cover foils. Sol Energy Mater Sol Cells 1995;37:93–118.
[10] Granqvist CG, Hjortsberg A, Eriksson TS. Radiative cooling to low temperatures with selectivity IR-emitting surfaces. Thin Solid Films 1982;90:187–90.
[11] Granqvist C, Hjortsberg A. Surfaces for radiative cooling: silicon monoxide films on aluminum. Appl Phys Lett 1980;36:139–41.
[12] Rephaeli E, Fan S. Absorber and emitter for solar thermo-photovoltaic systems to achieve efficiency exceeding the Shockley-Queisser limit. Opt Express 2009;17:15145–59.
[13] Yeng YX, Ghebrebrhan M, Bermel P, et al. Enabling high-temperature nanophotonics for energy applications. Proc Natl Acad Sci USA 2012;109:2280–5.
[14] Chan WR, Bermel P, Pilawa-Podgurski RCN, et al. Toward high-energy-density, high-efficiency, and moderate-temperature chip-scale thermophotovoltaics. Proc Natl Acad Sci USA 2013;110:5309–14.
[15] Joannopoulos JD, Johnson SG, Winn JN, Meade RD. Photonic crystals: molding the flow of light, 2nd ed. Princeton, NJ, Princeton University Press, 2008.
[16] Rephaeli E, Raman A, Fan S. Ultrabroadband photonic structures to achieve high-performance daytime radiative cooling. Nano Lett 2013;13:1457–61.
[17] Raman AP, Anoma MA, Zhu L, Rephaeli E, Fan S. Passive radiative cooling below ambient air temperature under direct sunlight. Nature 2014;515:540–4.
[18] Zhu L, Raman A, Wang KX, Anoma MA, Fan S. Radiative cooling of solar cells. Optica 2014;1:32–8.
[19] Zhu L, Raman AP, Fan S. Radiative cooling of solar absorbers using a visibly transparent photonic crystal thermal blackbody. Proc Natl Acad Sci USA 2015;112:12282–7.
[20] Wu S-H, Povinelli ML. Solar heating of GaAs nanowire solar cells. Opt Express 2015;23:A1363–72.
[21] Safi TTST, Munday JJN. Improving photovoltaic performance through radiative cooling in both terrestrial and extraterrestrial environments. Opt Express 2015;23:A1120–8.
[22] Sun X, Silverman TJ, Zhou Z, Khan MR, Bermel P, Alam MA. Optics-based approach to thermal management of photovoltaics: selective-spectral and radiative cooling. IEEE J Photovoltaics 2017;7:566–74.
[23] Francoeur M, Vaillon R, Menguc MP. Performance analysis of manoscale-gap thermophotovoltaic energy conversion devices. In the International Symposium on Thermal and Materials Nanoscience and Nanotechnology, Antalya, Turkey, 2011.
[24] Bermel P, Chan W, Yeng YX, Joannopoulos JD, Soljacic M, Celanovic I. Design and global optimization of high-efficiency thermophotovoltaic systems. In the 9th Thermophotovoltaic World Conf, Valencia, Spain, 2010.
[25] Thorne PW, Lanzante JR, Peterson TC, Seidel DJ, Shine KP. Tropospheric temperature trends: history of an ongoing controversy. Wiley Interdiscip Rev Clim Chang 2011;2:66–88.
[26] Vinnikov KY, Grody NC. Global warming trend of mean tropospheric temperature observed by satellites. Science 2003;302:269–72.
[27] Grant WB. Water vapor absorption coefficients in the 8-13 microm spectral region: a critical review: erratum. Appl Opt 1990;29:3206.
[28] Idso SB, Jackson RD. Thermal radiation from the atmosphere. J Geophys Res 1969;74:5397.
[29] Planck M. Ueber das gesetz der energieverteilung im normalspectrum. Ann Phys 1901;309:553–63.
[30] Greffet J-J, Bouchon P, Brucoli G, Sakat E, Marquier F. Generalized Kirchhoff law. arXiv preprint arXiv:1601.00312 (2016).
[31] Fixsen DJ. The temperature of the cosmic microwave background. Astrophys J 2009;707:916–20.
[32] US Standard Atmosphere. Report/patent number: NASA TM-X 74335. National Oceanic and Atmospheric Administration. Natl Aeronaut Sp Adm United States Air Force, 1976.
[33] ATRAN, 1992. [Online]. Available at: https://atran.sofia.usra.edu/cgi-bin/atran/atran.cgi. Accessed May 1, 2017.
[34] Bell EE, Young J, Oetjen RA. Spectral-radiance of sky and terrain at wavelengths between 1 and 20 microns. II. Sky measurements. J Opt Soc Am 1960;50:1313–20.
[35] McGee RA. An analytical infrared radiation model of the earth. Appl Opt 1962;1:649.
[36] Roberts RE, Selby JE, Biberman LM. Infrared continuum absorption by atmospheric water vapor in the 8-12-microm window. Appl Opt 1976;15:2085–90.
[37] Idso SB. A set of equations for full spectrum and 8- to 14-um and 10.5- to 12.5-um thermal radiation from cloudless skies. Water Resour Res 1981;17:295–304.
[38] Strabala KI, Ackerman SA, Menzel WP. Cloud properties inferred from 8-12-μm data. J Appl Meteorol 1994;33:212–29.
[39] Berdahl P, Fromberg R. The thermal radiance of clear skies. Sol Energy 1982;29:299–314.

[40] Harrison AW. Effect of atmospheric humidity on radiation cooling. Sol Energy 1981;26:243–47.
[41] Hossain MM, Gu M. Radiative cooling: principles, progress, and potentials. Adv Sci 2016;3:1500360.
[42] Berdahl P, Martin M, Sakkal F. Thermal performance of radiative cooling panels. Int J Heat Mass Transf 1983;26:871–80.
[43] Garratt JR, Brost RA. Radiative cooling effects within and above the nocturnal boundary layer. J Atmos Sci 1981;38:2730–46.
[44] Eicker U, Dalibard A. Photovoltaic-thermal collectors for night radiative cooling of buildings. Sol Energy 2011;85:1322–35.
[45] Artmann N, Manz H, Heiselberg P. Parameter study on performance of building cooling by night-time ventilation. Renew Energy 2008;33:2589–98.
[46] Holtslag AAM, De Bruin HAR. Applied modeling of the night-time surface energy balance over land. J Appl Meteorol 1988;27:689–704.
[47] Chen Z, Zhu L, Raman A, Fan S. Radiative cooling to deep sub-freezing temperatures through a 24-h day-night cycle. Nat Commun 2016;7:1–5.
[48] Nishioka K, Ota Y, Tamura K, Araki K. Heat reduction of concentrator photovoltaic module using high radiation coating. Surf Coat Technol 2013;215:472–5.
[49] Byrnes SJ, Blanchard R, Capasso F. Harvesting renewable energy from Earth's mid-infrared emissions. Proc Natl Acad Sci USA 2014;111:3927–32.
[50] Eriksson TS, Granqvist CG. Radiative cooling computed for model atmospheres. Appl Opt 1982;21:4381.
[51] Harrison AW, Walton MR. Radiative cooling of TiO_2 white paint. Sol Energy 1978:20:185–8.
[52] Grenier P. Réfrigération radiative. Effet de serre inverse. Rev Phys Appl 1979;14:87–90.
[53] Landro B, McCormick PG. Effect of surface characteristics and atmospheric conditions on radiative heat loss to a clear sky. Int J Heat Mass Transf 1980;23:613–20.
[54] Addeo A, Nicolais L, Romero G, Bartoli B, Coluzzi B, Silvestrini V. Light selective structures for large scale natural air conditioning. Sol Energy 1980;24:93–8.
[55] Eriksson TS, Granqvist CG. Infrared optical properties of electron-beam evaporated silicon oxynitride films. Appl Opt 1983;22:3204–6.
[56] Eriksson TS, Lushiku EM, Granqvist CG. Materials for radiative cooling to low temperature. Sol Energy Mater 1984;11:149–61.
[57] Eriksson TS, Granqvist CG. Infrared optical properties of silicon oxynitride films: experimental data and theoretical interpretation. J Appl Phys 1986;60:2081–91.
[58] Hjortsberg A, Granqvist CG. Radiative cooling with selectively emitting ethylene gas. Appl Phys Lett 1981:39:507–9.
[59] Lushiku EM, Hjortsberg A, Granqvist CG. Radiative cooling with selectively infrared-emitting ammonia gas. J Appl Phys 1982;53:5526–30.
[60] Suryawanshi CN, Lin C-T. Radiative cooling: lattice quantization and surface emissivity in thin coatings. ACS Appl Mater Interfaces 2009;1:1334–8.
[61] Gentle AR, Smith GB. Radiative heat pumping from the Earth using surface phonon resonant nanoparticles. Nano Lett 2010;10:373–9.
[62] Ghebrebrhan M, Bermel P, Yeng YX, Celanovic I, Soljačić M, Joannopoulos JD. Tailoring thermal emission via Q matching of photonic crystal resonances. Phys Rev A 2011;83:33810.
[63] Zhu L, Raman A, Fan S. Color-preserving daytime radiative cooling. Appl Phys Lett 2013;103:223902.
[64] Zhou Z, Sun X, Bermel P. Radiative cooling for thermophotovoltaic systems. Proc SPIE 2016;9973:997308.
[65] Granqvist CG, Hjortsberg A. Radiative cooling to low temperatures: general considerations and application to selectively emitting SiO films. J Appl Phys 1981;52:4205–20.
[66] Gentle AR, Smith GB. A subambient open roof surface under the mid-summer Sun. Adv Sci 2015;2:1500119.
[67] Taft EA. Characterization of silicon nitride films. J Electrochem Soc Solid State Sci 1971;118:1341.
[68] Pliskin WA. Comparison of properties of dielectric films deposited by various methods. J Vac Sci Technol 1977;14:1064.
[69] Gentle AR, Smith GB. Is enhanced radiative cooling of solar cell modules worth pursuing? Sol Energy Mater Sol Cells 2016;150:39–42.
[70] Granqvist CG, Hjortsberg A. Letter to the editor. Sol Energy 1980;24:216.
[71] Smith GB. Commentary: environmental nanophotonics and energy. J Nanophotonics 2011;5:50301.
[72] Bermel P, Luo C, Zeng L, Kimerling LC, Joannopoulos JD. Improving thin-film crystalline silicon solar cell efficiencies with photonic crystals. Opt Express 2007;15:16986–7000.
[73] Bermel P, Ghebrebrhan M, Chan W, et al. Design and global optimization of high-efficiency thermophotovoltaic systems. Opt Express 2010;18:A314–34.
[74] Zhou Z, Chen Q, Bermel P. Prospects for high-performance thermophotovoltaic conversion efficiencies exceeding the Shockley-Queisser limit. Energy Convers Manag 2015;97:63–9.
[75] Eriksson TSS, Hjortsberg A, Granqvist CGG. Solar absorptance and thermal emittance of Al_2O_3 films on Al: a theoretical assessment. Sol Energy Mater 1982;6:191–9.
[76] Strandberg R. Heat to electricity conversion by cold carrier emissive energy harvesters. J Appl Phys 2015;118:215102.
[77] Otth DH, Ross, RGJ. Assessing photovoltaic module degradation and lifetime from long term environmental tests. In Environmental technology: a key to product acceptability. Annual Technical Meeting, Los Angeles, CA, 1983, Vol. 29, 121–6.
[78] Bermel P, Asadpour R, Zhou C, Alam MA. A modeling framework for potential induced degradation in PV modules. Proc SPIE 2015;9563:95630C-95630C.
[79] Asadpour R, Chavali RVK, Alam MA. Physics-based computational modeling of moisture ingress in solar modules: location-specific corrosion and delamination. In 2016 IEEE 43rd Photovoltaic Specialists Conference (PVSC), Portland, OR, 2016, 0840–3.
[80] NREL Efficiency Chart, 2016. [Online]. Available at: http://www.nrel.gov/pv/assets/images/efficiency_chart.jpg. Accessed May 1, 2017.
[81] Gregory MK, Shuying Y, Ajay S. Global acceleration factors for damp heat tests of PV modules. In IEEE 43rd Photovoltaic Specialist Conference (PVSC), Portland, OR, 2016.
[82] Royne A, DEY CJ, Mills DR. Cooling of photovoltaic cells under concentrated illumination: a critical review. Sol Energy Mater Sol Cells 2005;86:451–83.
[83] Edenburn MW. Active and passive cooling for concentrating photovoltaic arrays. In IEEE 14th Photovoltaic Specialist Conference (PVSC), San Diego, CA, 1980, 771–776.

[84] Koehler HC. Cooling photovoltaic (PV) cells during concentrated solar radiation in specified arrangement in coolant with as low electric conductivity as possible. Patent DE19904717, 2000.
[85] Florschuetz LW, Truman CR, Metzger DE. Streamwise flow and heat transfer distributions for jet array impingement with crossflow. J Heat Transfer 1981;103:337.
[86] Corkish R, Green MA, Puzzer T. Solar energy collection by antennas. Sol Energy 2002;73:395–401.
[87] Vandenbosch GAE, Ma Z. Upper bounds for the solar energy harvesting efficiency of nano-antennas. Nano Energy 2012;1:494–502.
[88] Ward DR, Hüser F, Pauly F, Cuevas JC, Natelson D. Optical rectification and field enhancement in a plasmonic nanogap. Nat Nanotechnol 2010;5:732–6.
[89] Knight MW, Sobhani H, Nordlander P, Halas NJ. Photodetection with active optical antennas. Science 2011;332:702–4.
[90] Hobbs PCD, Laibowitz RB, Libsch FR. Ni-NiO-Ni tunnel junctions for terahertz and infrared detection. Appl Opt 2005;44:6813.
[91] Kotter DK, Novack SD, Slafer WD, Pinhero PJ. Theory and manufacturing processes of solar nanoantenna electromagnetic collectors. J Sol Energy Eng 2010;132:11014.
[92] Fumeaux C, Herrmann W, Kneubühl FK, Rothuizen H. Nanometer thin-film Ni-NiO-Ni diodes for detection and mixing of 30 THz radiation. Infrared Phys Technol 1998;39:123–83.
[93] Hagmann MJ. Isolated carbon nanotubes as high-impedance transmission lines for microwave through terahertz frequencies. IEEE Trans Nanotechnol 2005;4:289–96.
[94] Choo H, Kim M-K, Staffaroni M, et al. Nanofocusing in a metal-insulator-metal gap plasmon waveguide with a three-dimensional linear taper. Nat Photonics 2012;6:838–44.
[95] Conibeer G, Shrestha S, Huang S, et al. Hot carrier solar cell absorber prerequisites and candidate material systems. Sol Energy Mater Sol Cells 2015;135:124–9.
[96] Würfel P, Brown AS, Humphrey TE, Green MA. Particle conservation in the hot-carrier solar cell. Prog Photovoltaics Res Appl 2005;13:277–85.
[97] Santhanam P, Fan S. Thermal-to-electrical energy conversion by diodes under negative illumination. Phys Rev B 2016;93:161410.
[98] Tan Y, Liu B, Shen S, Yu Z. Enhancing radiative energy transfer through thermal extraction. Nanophotonics 2016;5:22–30.
[99] Kempfert KD, Jiang EY, Oas S, Coffin J. Detectors for Fourier transform spectroscopy. Thermo Nicolet Application Note. [Online]. Available at: mmrc.caltech.edu/FTIR/Nicolet/DetectorsforFTIR1204.pdf. Accessed May 1, 2017.
[100] Asgari A, Razi S. High performances III-Nitride Quantum Dot infrared photodetector operating at room temperature. Opt Express 2010;18:14604.
[101] Datskos PC, Lavrik N V. Detectors – figures of merit. In Encyclopedia of Optical Engineering. CRC Press, 2003.
[102] Jiang H, Shin S, Liu X, Zhang X, Alam MA. Characterization of self-heating leads to universal scaling of HCI degradation of multi-fin SOI FinFETs. In 2016 IEEE International Reliability Physics Symposium (IRPS), Pasadena, CA, 2016, 2A-3-1–7.
[103] Maize K, Das SR, Sadeque S, et al. Super-Joule heating in graphene and silver nanowire network. Appl Phys Lett 2015;106:143104.
[104] Palit S, Varghese D, Guo H, Krishnan S, Alam MA. The role of dielectric heating and effects of ambient humidity in the electrical breakdown of polymer dielectrics. IEEE Trans Device Mater Reliab 2015;15:308–18.
[105] Wahab MA, Shin S, Alam MA. Spatio-temporal mapping of device temperature due to self-heating in Sub-22 nm transistors. In 2016 IEEE International Reliability Physics Symposium (IRPS), Pasadena, CA, 2016, XT-05-1–6.
[106] Shin SH, Wahab MA, Ahn W, et al. Fundamental trade-off between short-channel control and hot carrier degradation in an extremely-thin silicon-on-insulator (ETSOI) technology. In 2015 IEEE International Electron Devices Meeting (IEDM), Washington, DC, 2015, 20.3.1–4.
[107] Alam MA, Mahapatra S. A comprehensive model of PMOS NBTI degradation. Microelectron Reliab 2005;45:71–81.
[108] Cheng Y-K, Tsai C-H, Teng C-C, Kang S-M. Electrothermal Analysis of VLSI Systems, Springer Science & Business Media, 2007, Chapter 6.
[109] Viswanath R, Wakharkar V, Watwe A, Lebonheur V. Thermal performance challenges from silicon to systems. Intel Technol J 2000:1–16. http://citeseerx.ist.psu.edu/viewdoc/summary?doi=10.1.1.14.8322.
[110] Berhe MK. Ergonomic temperature limits for handheld electronic devices. In ASME 2007 InterPACK Conference, Vancouver, BC, Canada, 2007, Vol. 2, 1041–7.
[111] Wagner GR, Maltz W. Comparing tablet natural convection cooling efficiency. [Online]. Available at: https://www.mentor.com/products/mechanical/engineering-edge/volume3/issue1/comparing-natural-convection-cooling-efficiency. Accessed May 1, 2017.
[112] Yu E, Joshi YK. Heat transfer in discretely heated side-vented compact enclosures by combined conduction, natural convection, and radiation. J Heat Transfer 1999;121:1002.
[113] De Vogeleer K, Memmi G, Jouvelot P, Coelho F. Theoretical analysis of radiative cooling for mobile and embedded systems. arXiv preprint arXiv:1410.0628 (2014).